A TIME-REVERSAL SPATIAL HARDENING EFFECT FOR INDOOR SPEED ESTIMATION

Feng Zhang[⋆†], *Chen Chen*[⋆†], *Beibei Wang*[⋆†∗], *Hung-Quoc Lai*[⋆∗] *and K. J. Ray Liu*[⋆†]

[⋆]Origin Wireless Inc., 7500 Greenway Center Drive, Suite 1070, MD 20770, USA.
[†]University of Maryland, College Park, MD 20742, USA.
Email: {fzhang15, cc8834, kjrliu}@umd.edu[†], {beibei.wang, quoc.lai}@originwireless.net[∗]

ABSTRACT

Time-reversal (TR) transmission scheme has attracted more and more attention from both academia and industry due to its ability to focus the energy of a transmitted signal at an intended focal spot, both in the time and spatial domains. Based on the extensive data collected in the real world, we observe that the energy distribution around the focal spot is highly stationary and location-independent, which we call as the "TR spatial hardening effect". This is because TR scheme adds up numerous copies of the transmitted signal bouncing off different scatterers coherently and the randomness from the environment is averaged out. We characterize the statistical behaviors of the energy distribution around the focal spot using a statistical model. By exploiting the hardening effect, the moving speed of transceivers can be estimated in indoor environments and extensive experiments show the superiority of the proposed method compared with previous works using RF signals.

***Index Terms*—** indoor speed estimation, spatial hardening effect, time-reversal

1. INTRODUCTION

Time-reversal resonating effect is a fundamental physical resonance phenomenon that can focus the energy of a transmitted signal at an intended focal spot both temporally and spatially. The research of TR dates back to the 1950s, where TR was utilized to align the phase differences caused by multipath fading during long-distance information transmissions [1], and the resonating effect was also observed in a practical underwater propagation environment [2]. The capacity of TR technology in refocusing the energy in the vicinity of an intended focal spot at a particular moment enables wide applications of TR techniques in acoustic communications [3], wireless communications [1, 4, 5, 6], and indoor positioning systems [7, 8].

TR scheme enjoys its elegant simplicity as it harvests energy from the surrounding environment by exploiting the multipath propagation, giving rise to the well-known TR resonating effect. The TR resonating effect has been well studied in theory under very strong assumptions on the propagation medium such as homogeneity and discrete scattering [9, 10, 11]. It is studied via numerical simulations an experiments in controlled environments, for instance, reverberation chambers consisting of metallic walls [12, 13, 14]. Recently, H. El-Sallabi *et al.* conducted an experiment in an indoor space with 240 MHz bandwidth [15]. However, they investigate the spatial focusing effect at one fixed location and only with a resolution of half-wavelength, far from enough to fully unveil the details of the energy distribution of the received signal within the focal spot. In addition, only a single realization of the received energy around the focal spot was measured which fails to shed light on the statistical behaviors of the energy distribution.

To investigate the energy distribution within the focusing ball, we collect the channel impulse responses (CIR) extensively in real-world rich-scattering environments with a much finer measurement resolution. We observe that the energy distribution inside the focusing ball is highly stationary and location-independent. We call such a phenomenon as the TR spatial hardening effect. Using the measurement data, we develop a statistical model to explain the observed TR hardening phenomenon.

Further, this location-independent characteristic can be applied in indoor speed estimation, since the decay of the received energy can be translated to the distance away from the focal spot. Traditional methods for speed estimation based on Doppler shift fails to track (human walking) speed when RF signals are reflected by numerous scatterers in typical indoor environments and when the speed is too slow to produce perceptible Doppler shift. Other schemes such as the inertial sensor based schemes [16] and the coherence time based method [17] cannot perform well either since they are generally based on the strong assumption of uniform walking speed. Using the location-independent characteristic of TR resonating effect, the proposed speed estimation algorithm can produce accurate estimations in a complicated indoor environment using RF signals even when the speed is low and non-uniform, which have been validated through experiments.

The rest of the paper is organized as follows. Section 2 describes the TR transmission scheme and shows the TR resonating effect obtained from measurement data using our own

platform. TR spatial hardening effect is presented in Section 3 followed by statistical explanations. Section 4 presents a TR-based indoor speed estimation algorithm and the experiment results. Finally, conclusion is drawn in Section 5.

2. PRELIMINARIES

2.1. TR Transmission Scheme

Consider a radio rich-scattering environment, i.e., it can be either indoor or metropolitan area. Consider a wireless transceiver pair each equipped with a single omnidirectional antenna in a rich-scattering environment. Given a large enough bandwidth, the MPCs in a rich-scattering environment can be resolved into multiple taps in discrete-time and let $h(k; \vec{T} \rightarrow \vec{R}_0)$ denote the k-th tap of the CIR from $\vec{T}$ to $\vec{R}_0$, where $\vec{T}$ and $\vec{R}_0$ denotes the coordinates of the transmitter and receiver, respectively. In the TR transmission scheme, the receiver at $\vec{R}_0$ first transmits an impulse and the transmitter at $\vec{T}$ captures the CIR from $\vec{R}_0$ to $\vec{T}$. Then the transmitter at $\vec{T}$ simply transmits back the reversed and conjugated version of the captured CIR, i.e., $h^*(-k; \vec{R}_0 \rightarrow \vec{T})$, where $*$ denotes complex conjugation. In the following, $\vec{R}_0$ is called the focal spot. Without loss of generality, we use $h(k; \vec{R})$ instead of $h(k; \vec{R}_0 \rightarrow \vec{T})$ when $\vec{T}$ is fixed. With the channel reciprocity, i.e., the forward and backward channel are identical which has been verified experimentally [8], the received signal at $\vec{R}$ can be written as

$$s(k; \vec{R}) = \sum_{l=0}^{L-1} h(l; \vec{R}) h^*(l-k; \vec{R}_0), \tag{1}$$

where L is the length of the CIR, $h(l-k; \vec{R}_0) = 0$ when $(l-k) \notin \{0, 1, ..., L-1\}$, and $k \in \{-(L-1), ..., (L-1)\}$. When $\vec{R} = \vec{R}_0$ and $k = 0$, $|s(k; \vec{R})|$ attains the maximum value $\sum_{l=0}^{L-1} |h(l, R)|^2$ when all MPCs are accumulated coherently, i.e., the signal energy is refocused on one particular spatial location at one specific time instance. This phenomenon is termed as the TR spatial-temporal resonating effect. To study the TR resonating effect in the spatial domain, we fix $k = 0$ and define the TR resonating strength (TRRS) as the normalized received signal energy at $\vec{R}$, given by

$$\eta(\mathbf{h}(\vec{R}_0), \mathbf{h}(\vec{R})) = \left| \frac{s(0; \vec{R})}{\sqrt{\sum_{l=0}^{L-1} |h(l; \vec{R}_0)|^2} \sqrt{\sum_{l=0}^{L-1} |h(l; \vec{R})|^2}} \right|^2, \tag{2}$$

assuming the transmitter simply transmits back the time reversed and conjugated version of $\vec{R}_0$.

2.2. Energy Distribution in TR Resonating Effect

To understand the TR spatial-temporal resonating effect as well as to study the spatial distribution of TRRS with a fine granularity, we conduct extensive experiments in a typical indoor environment using customized TR devices operating at 5GHz ISM band with 125MHz bandwidth. The TR transmitter is placed at an NLOS position with no direct path between the transmitter and the receiver, as shown in Fig. 1 and the TR receiver is placed on the channel probing platform. CIRs corresponding to the locations from a square area with dimension 5cm $\times$ 5cm are measured and the measurement resolution is 0.5cm. In total, 121 CIRs are captured. In Fig. 2, we demonstrate the TRRS at different locations when the focal spot $\vec{R}_0$ is located in the middle of the square area. As we can observe, TRRS is very close to 1 in the vicinity of $\vec{R}_0$, indicating a very high similarity in CIRs between the locations very close to $\vec{R}_0$, but decays rapidly when the distance to $\vec{R}_0$ increases. This observation illustrates the energy distribution of the TR spatial resonating effect around a focal spot for a single realization.

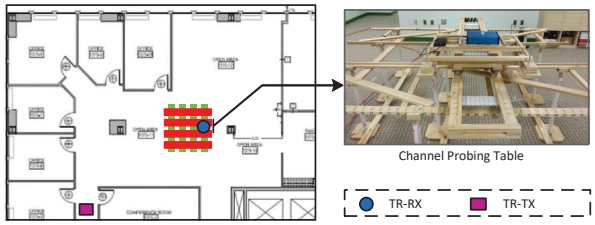

Fig. 1. TR system prototypes and channel probing platform.

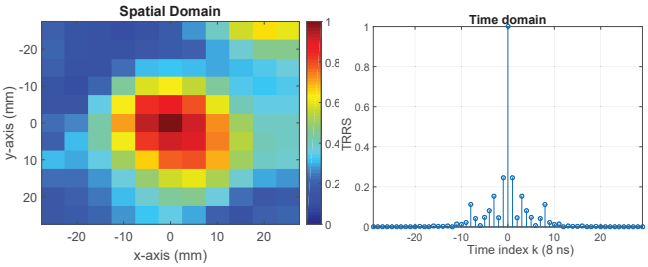

(a) Spatial resonating effect (b) Temporal resonating effect

Fig. 2. TR resonating effect in spatial and time domains.

3. TR SPATIAL HARDENING EFFECT

3.1. Experiment Setup and Observations

In order to investigate the energy distribution around different focal spots, we randomly choose 55 locations on the channel probing platform as different focal spots. The shortest distance between any two focal spots is 20cm. For each focal spot $\vec{R}_0$, we measure the CIRs from 20 equally-spaced locations with a resolution of 0.5cm lying on the same straight

line with $\vec{R}_0$. For each $\vec{R}_0$, we calculate the TRRS between the CIRs obtained at $\vec{R}_0$ and those associated with nearby locations. Then, we plot the TRRS decay curve which depicts the impact of distance on TRRS. In Fig. 3, we demonstrate an ensemble composed by 55 TRRS decay curves as well as the TRRS variance at different distances. The results imply that the TRRS decreases rapidly with the distance d and saturates when $d \geq 20$mm. Meanwhile, the TRRS variance is very small near the focal spot, indicating that the TRRS is predictable when the distance between the focal spot and the location is sufficiently small. Based on this observation, we

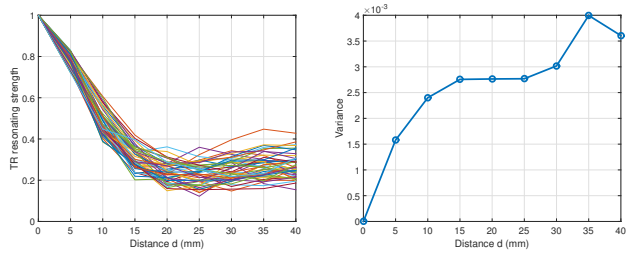

(a) TRRS decays w.r.t. d (b) Sample variances w.r.t. d

Fig. 3. TRRS decay curves from 55 different focal spots.

define the TR spatial hardening effect as follows: in a rich-scattering environment and given a sufficiently large bandwidth, time-reversal can focus the energy around the focal spot in a highly predictable way.

3.2. Statistical Modeling of TR Resonating Effect

Now we treat the CIR as a random vector denoted as $\mathbf{H}$ and thus $\mathbf{h}(\vec{R})$ can be treated as a realization of $\mathbf{H}$ at location $\vec{R}$. We use $\mathbf{H}(l)$ to denote the l-th element of $\mathbf{H}$ where $l = 0, 1, ..., L-1$. Let $(\mathbf{H}, \mathbf{H}_d)$ denote the pair of CIR random vectors with distance d apart from each other, and a realization of $(\mathbf{H}, \mathbf{H}_d)$ at location $(\vec{R}_0, \vec{R}_0 + \vec{\Delta})$ can be presented as $\left(\mathbf{h}(\vec{R}_0), \mathbf{h}(\vec{R}_0 + \vec{\Delta})\right)$ for any $\|\vec{\Delta}\|_2 = d$. Based on the CIR measurements, we conclude:

Fact 1. $\mathbf{H}(l)$ *is a complex Gaussian random variable, distributed as* $\mathcal{CN}(0, \sigma_0^2 e^{-\alpha l})$, $\forall l = 0, 1, ..., L-1$. [1]

Fact 2. $\mathbf{H}(l)$ *and* $\mathbf{H}(k)$ *are independent,* $\forall l \neq k$.

We use the sample correlation $\rho\left(\mathbf{H}(l), \mathbf{H}_d(k)\right)$ as the metric to quantify the correlation between $\mathbf{H}(l)$ and $\mathbf{H}_d(k)$, which is defined as

$$\rho\left(\mathbf{H}(l), \mathbf{H}_d(k)\right) = \frac{\sum_{i=1}^{N} \left(\mathbf{h}^{(i)}(l) - \bar{\mathbf{h}}(l)\right)^* \left(\mathbf{h}_d^{(i)}(k) - \bar{\mathbf{h}}_d(k)\right)}{\left[\left(\sum_{i=1}^{N} \left|\mathbf{h}^{(i)}(l) - \bar{\mathbf{h}}(l)\right|^2\right)\left(\sum_{i=1}^{N} \left|\mathbf{h}_d^{(i)}(l) - \bar{\mathbf{h}}_d(l)\right|^2\right)\right]^{\frac{1}{2}}}, \quad (3)$$

[1] α equals to 0.1952 in our typical indoor environment.

where N is the number of samples, $\mathbf{h}^{(i)}(l)$ stands for the l-th component of the i-th sample pair and $\bar{\mathbf{h}}(l)$ is defined as the sample mean, i.e., $\bar{\mathbf{h}}(l) \triangleq \sum_{i=1}^{N} \mathbf{h}^{(i)}(l)$. The results in Fig. 4 show that the correlation only exists between the taps with the same index and correlations coefficients with $l = k \geq 4$ are almost the same for fixed distance value d. The first three taps are more correlated than the others since they correspond to the reflectors near the focal spot, which contain a significant channel energy from the line-of-sight (LoS) MPC. In addition, we also note that the correlation coefficients decay rapidly when d increases and the correlations become negligible when $d = 20$mm.

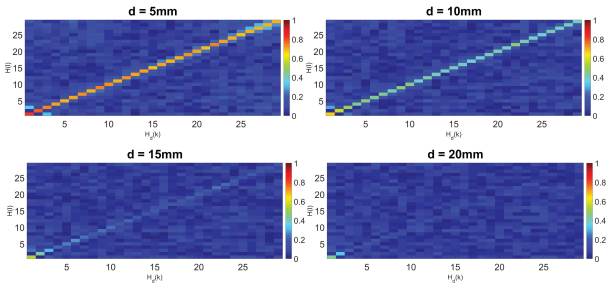

Fig. 4. Correlation coefficient matrix $|\rho\left(\mathbf{H}(l), \mathbf{H}_d(k)\right)|$.

Based on these observations, we have the following assumptions for modeling the spatial correlation among CIRs from nearby locations.

Assumption 1. $(\mathbf{H}, \mathbf{H}_d)$ *are joint Gaussian random vectors with a diagonal covariance matrix.*

Assumption 2. $\rho_d = \frac{\mathbb{E}[\mathbf{H}_d(l)\mathbf{H}^*(l)]}{\sigma_l^2}$, $\forall l = 0, 1, ..., L-1$, *where* $\mathbb{E}$ *stands for the expectation operator.*

If the TR transmission scheme is applied, then the received signal for the location with distance d away from the focal spot at time k is also a random variable (RV) S as follows:

$$S(k; d) = \sum_{l=0}^{L-1} \mathbf{H}_d(l)\mathbf{H}^*(l-k), \quad (4)$$

where $\mathbf{H}(l-k) = 0$ when $(l-k) \notin \{0, 1, ..., L-1\}$ and $k \in \{-(L-1), ..., (L-1)\}$. Let $\eta(d)$ denote the TRRS between $\mathbf{H}$ and $\mathbf{H}_d$, i.e., $\eta(d) \triangleq \eta(\mathbf{H}, \mathbf{H}_d)$, and we call $\eta(d)$ as the TR spatial resonating decay function. Under Assumption 1-2, $\bar{\eta}(d) \triangleq \mathbb{E}[\eta(d)]$ can be approximated by taking the expectation operations to the numerator and denominator of $\eta(d) = \left|\frac{S(0;d)}{\|\mathbf{H}\|_2 \|\mathbf{H}_d\|_2}\right|^2$, respectively, as follows [6]:

$$\mathbb{E}[|S(0;d)|^2] = \sigma_0^4 \left(\frac{1 - e^{-2\alpha L}}{1 - e^{-2\alpha}} + |\rho_d|^2 \left(\frac{1 - e^{-\alpha L}}{1 - e^{-\alpha}}\right)^2\right); \quad (5)$$

$$\mathbb{E}[\|\mathbf{H}\|_2^2\|\mathbf{H}_d\|_2^2] = \sigma_0^4\left(|\rho_d|^2\frac{1-e^{-2\alpha L}}{1-e^{-2\alpha}} + \left(\frac{1-e^{-\alpha L}}{1-e^{-\alpha}}\right)^2\right). \quad (6)$$

The average of the TR spatial resonating decay function $\eta(d)$ can be obtained from the measured data and the joint Gaussian approximations [2] respectively as shown in Fig. 5. The result shows that the proposed approximations match the experiment result well with respect to the TR spatial resonating decay function, which indicates that the approximations can indeed capture the essential characteristics of the TR spatial resonating effect. Given a realization of the CIR at the focal

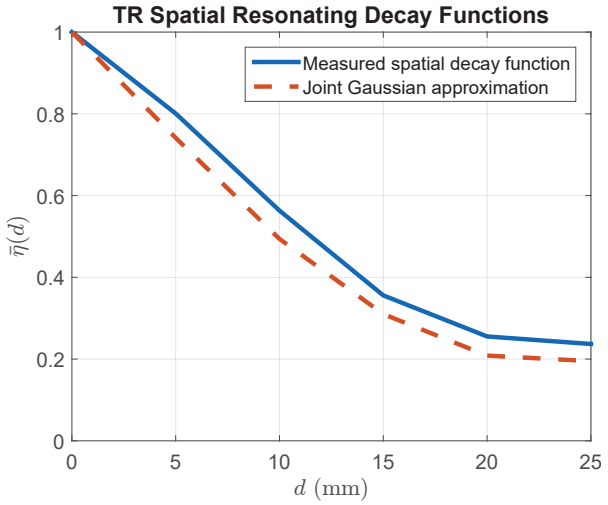

Fig. 5. The average of TR spatial resonating decay function.

spot $\mathbf{H} = \mathbf{h}$, the variance of the received signal $S(0;d)$ is

$$\text{Var}[S(0;d)|\mathbf{H}=\mathbf{h}] = \sigma_0^2(1-|\rho_d|^2)\mathbf{h}'\mathbf{\Lambda}\mathbf{h}, \quad (7)$$

where Λ is a diagonal matrix with the (k,k)-th element given as $e^{-\alpha(k-1)}$. For locations in the close vicinity of the focal spot, the variance of the received signal energy is also small since $|\rho_d|$ is close to 1. Given a larger bandwidth, σ_0^2 decreases since the total channel power gain distributes among a larger number of taps, which will further decrease the variance of $S(0;d)$. Therefore, the TR spatial hardening effect only happens when the bandwidth is large enough.

4. TR-BASED SPEED ESTIMATION

The TR transceiver pair is placed in an NLOS scenario and CIRs are measured constantly with a channel probing rate of 100Hz. The core idea of the algorithm is to translate the reduction in the resonating strength into the moving distance of the TR transmitter or receiver. In addition, we use an averaging window with length N to further mitigate the fluctuations of the TR spatial resonating decay function.

[2]The correlation coefficients are obtained from the measured CIRs.

Algorithm 1 TR indoor speed estimation

Input: The most recent N CIRs: $[\mathbf{h}_{t-N+1}, ..., \mathbf{h}_t]$
Output: Speed estimation at time t: $\hat{v}(t)$

1: Initialization: $\Sigma \leftarrow 0$, T_s (channel probing interval)
2: **for** $i \in \{t-N+1, ..., t-1\}$ **do**
3: $\quad \Sigma \leftarrow \Sigma + \eta(\mathbf{h}_i, \mathbf{h}_{i+1})$
4: **end for**
5: $\hat{v}(t) = \frac{\bar{\eta}^{-1}(\Sigma/(N-1))}{T_s}$

To evaluate the performance of the speed estimation scheme, we conduct two experiments as follows. (i) In the first experiment, one participant carries the TR transmitter and walks at 0.5m/s. (ii) We fasten the TR transmitter to the end of a $R = 2.17$ meters long string and the other end of the string is tied to the ceiling. We release the string at an angle of $\theta = 0.22$ rads with respect to the vertical direction. The theoretical speed of the TR transmitter at time t can be computed as $v(t) = \theta\omega R\cos(\omega t + \phi)$, where $\omega = \sqrt{g/R}$, g is the gravitational acceleration, and ϕ is the initial phase. The experimental results in Fig. 6 shows that the proposed speed estimation algorithm can work very well in both slow human-walking and fast-changing speed settings. One thing to note is that the result is independent of the specific locations of the TR receiver even when the transceiver pair is placed in an NLOS setting which indicates that the TR spatial hardening effect is indeed uniform in typical indoor environments.

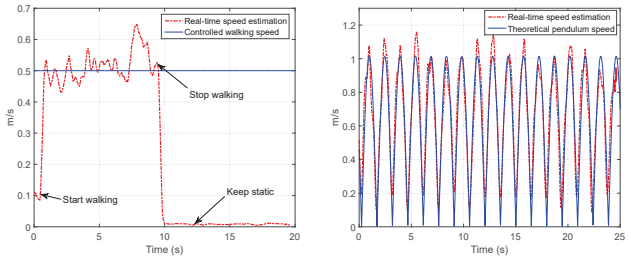

(a) Walking speed estimation (b) Pendulum speed estimation

Fig. 6. Experiment results of real-time speed estimations of the two cases.

5. CONCLUSIONS

In this paper, we present a statistical model of TRRS in close proximity to the focal spot to depict the TR spatial hardening effect based on extensive experiment results in an indoor environment with fine granularity measurement. Leveraging the TR spatial hardening effect, we present a TR-based indoor speed estimation scheme with high accuracy in an indoor environment.

6. REFERENCES

[1] C. Yan, B. Wang, Y. Han et al., "Why Time Reversal for Future 5G Wireless?," in *IEEE Signal Processing Magazine*, 33(2):17–26, 2016.

[2] P. Roux, B. Roman and M. Fink, "Time-reversal in an ultrasonic waveguide," in *Applied Physics Letters*, 70(14):1811–1813, 1997.

[3] M. Fink, "Time-reversed acoustics," in *Scientific American*, 281(5):91–97, 1999.

[4] M. Emami, M. Vu, J. Hansen, A.J. Paulraj and G. Papanicolaou, "Matched filtering with rate back-off for low complexity communications in very large delay spread channels," in *Proceedings of the Thirty-Eighth Asilomar Conference on Signals, Systems and Computers*, 218–222, 2004.

[5] B. Wang, Y. Wu, F. Han, Y. Yang and K.J. Liu, "Green wireless communications: A time-reversal paradigm," in *IEEE Journal on Selected Areas in Communications*, 29(8):1698–1710, 2011.

[6] F. Han, Y. Yang, B. Wang et al., "Time-reversal division multiple access over multi-path channels," in *IEEE Transactions on Communications*, 60(7):1953–1965, 2012.

[7] C. Chen, Y. Chen, H.Q. Lai, Y. Han and K.J.R. Liu, "High Accuracy Indoor Localization: A WiFi-Based Approach," in *Proceedings of IEEE International Conference on Acoustics, Speech and Signal Processing (ICASSP)*, 2016.

[8] Z.H. Wu, Y. Han et al., "A time-reversal paradigm for indoor positioning system," in *IEEE Transactions on Vehicular Technology*, 64(4): 1331–1339, 2015.

[9] C. Oestges, A.D. Kim et al., "Characterization of space-time focusing in time-reversed random fields," in *IEEE Transactions on Antennas and Propagation*, 53(1): 283–292, 2005.

[10] J. De Rosny, G. Lerosey and M. Fink, "Theory of electromagnetic time-reversal mirrors," in *IEEE Transactions on Antennas and Propagation*, 58(10): 3139–3149, 2010.

[11] L. Borcea, G. Papanicolaou, and C. Tsogka, "Theory and applications of time reversal and interferometric imaging," in *Inverse Problems* 19(6):139–164, 2003.

[12] G. Lerosey, J. De Rosny, A. Tourin and M. Fink, "Focusing beyond the diffraction limit with far-field time reversal," in *Science*, 315(5815): 1120–1122, 2007.

[13] G. Lerosey, J. De Rosny, A. Tourin, A. Derode and M. Fink, "Time reversal of wideband microwaves," in *Applied Physics Letters*, 88(15): 154101–154101, 2006.

[14] G. Lerosey, J. De Rosny, A. Tourin, A. Derode, G. Montaldo, and M. Fink, "Time reversal of electromagnetic waves and telecommunication," in *Radio Science*, 40(6), 2005.

[15] H. El-Sallabi, P. Kyritsi, A. Paulraj, and G. Papanicolaou, "Experimental investigation on time reversal precoding for spacetime focusing in wireless communications," in *IEEE Transactions on Instrumentation and Measurement*, 59(6): 1537–1543, 2010.

[16] Z. Yang, C. Wu, Z. Zhou, X. Zhang, X. Wang and Y. Liu, "Mobility increases localizability: A survey on wireless indoor localization using inertial sensors," in *ACM Computing Surveys (CSUR)*, 47(3): 54, 2015.

[17] B. Pricope, and H. Haas, "Experimental validation of a new pedestrian speed estimator for OFDM systems in indoor environments," in *the Proceedings of IEEE Global Telecommunications Conference*, 2011.